Physical immobilization of particles inspired by pollination

Lúcia F. Santos[a,1], A. Sofia Silva[a,1], Clara R. Correia[a], and João F. Mano[a,2]

[a]Department of Chemistry, CICECO–Aveiro Institute of Materials, University of Aveiro, 3810-193 Aveiro, Portugal

Edited by David Quéré, Ecole Supérieure de Physique et de Chimie Industrielles, Paris, France, and accepted by Editorial Board Member Pablo G. Debenedetti January 25, 2019 (received for review August 2, 2018)

Biomimetic systems often exhibit striking designs well adapted to specific functions that have been inspiring the development of new technologies. Herein, we explored the remarkable ability of honey bees to catch and release large quantities of pollen grains. Hair spacing and height on bees are crucial for their ability to mechanically fix pollen grains. Inspired by this, we proposed the concept of a micropatterned surface for microparticle entrapment, featuring high-aspect-ratio elastic micropillars spaced to mimic the hairy surface of bees. The hypothesis was validated by investigating the ability of polydimethylsiloxane microfabricated patches to fix microparticles. The geometrical arrangement, spacing, height, and flexibility of the fabricated micropillars, and the diameter of the microparticles, were investigated. Higher entrapment capability was found through the match between particle size and pillar spacing, being consistent with the observations that the diameter of pollen grains is similar to the spacing between hairs on bees' legs. Taller pillars permitted immobilization of higher quantities of particles, consistent with the high aspect ratio of bees' hairs. Our biomimetic surfaces were explored for their ability to fix solid microparticles for drug-release applications, using tetracycline hydrochloride as a model antibiotic. These surfaces allowed fixation of more than 20 mg/cm^2 of antibiotic, about five times higher dose than commercialized patches (5.1 mg/cm^2). Such bioinspired hairy surfaces could find applications in a variety of fields where dry fixation of high quantities of micrometer-sized objects are needed, including biomedicine, agriculture, biotechnology/chemical industry, and cleaning utensils.

biomimetic | drug carriers | honey bee | patches | pollination

The unique features exhibited by biological organisms in nature have been a source of inspiration for the development of high-performance structures and biomaterials (1). The emerging field of biomimetics has enabled the fabrication of novel soft materials and functional surfaces based on an understanding of natural designs and processes, providing solutions to challenges in the fields of engineering, materials science, and biomedicine (2–4).

Superhydrophobicity, self-cleaning, high and reversible adhesion, mechanical toughness, and self-healing are some of the numerous properties found in nature and subsequently employed in the development of high-performance surfaces and hydrogels (2, 5). More specifically, biomimetic adhesives have been inspired by geckos, beetles, flies, and other animals with the ability to strongly and reversibly adhere to surfaces. This capacity relies on the surface topography of their attachment pads (6), which are covered with a pattern of microstructures, resembling the geometry of tenent hairs present on their feet (7).

The peculiar hairy structure that covers the surface of the legs of honey bees allows them to fix and carry millions of pollen particles (Fig. 1*A*). Such insects have a typical hairy structure with numerous short lateral barbs with the length of 250 μm and hair radius of 10 μm. The pollen grains, which are of a similar diameter to the spacing between the hairs (~30 μm), are entrapped and temporarily retained, only being released on movement of the creature's leg (8–10). Replicating this natural structure using microfabrication could provide a substrate to be used in a wide variety of applications that require simple, nonpermanent, high-content, and purely physical immobilization of solid particulate objects (Fig. 1 *B* and *C*).

Drug-delivery systems are one such potential application of these biomimetic substrates (11). Transdermal drug delivery has been exploited as a successful controlled drug-release platform that has received regulatory approval, with several products now available on the market (12). Drug patches with diverse designs have been developed, ranging from passive drug delivery with little/no permeation enhancement to complex systems that enable the delivery of small molecules and macromolecules (13). However, passive-delivery patches have been beset by problems limiting their application (14, 15), with one potential solution being a higher drug content to improve transcutaneous fluxes (16). Herein, we show the development of a hierarchical biomimetic patch consisting of a polydimethylsiloxane (PDMS) micropatterned pillar structure and investigate the entrapment of polycaprolactone (PCL) microparticles. In addition, as a proof-of-concept, alginate microparticles were loaded with tetracycline, a broad-spectrum antibiotic (17), and their entrapment and subsequent antibacterial activity was evaluated.

Results

Fabrication of PDMS Micropatterned Patches. To explore the remarkable ability of honey bees to fix microsized pollen grains during pollination, different constructs that mimic the hairy surface of bees were fabricated to investigate their ability to catch and release spherical-shaped microparticles. PDMS micropatterned

Significance

Honey bees present a peculiar hairy structure that covers the surface of their body, which is able to transport large quantities of pollen particles for pollination purposes. Inspired by this natural phenomenon and to overcome the current problems associated with drug patches with passive delivery, we propose the concept of a micropatterned surface featuring micropillars with defined spacing and height to mimic the hair of bees for the entrapment of a large quantity of microparticles. We believe that such substrates could be extended to diverse applications that require reversible immobilization of solid particulate objects. In particular, high drug content is required for obtaining more effective drug patches, enabling more sustained and targeted release of the drug.

Author contributions: L.F.S., A.S.S., and J.F.M. designed research; L.F.S. and A.S.S. performed research; C.R.C. contributed new reagents/analytic tools; and L.F.S., A.S.S., C.R.C., and J.F.M. wrote the paper.

The authors declare no conflict of interest.

This article is a PNAS Direct Submission. D.Q. is a guest editor invited by the Editorial Board.

[1]L.F.S. and A.S.S. contributed equally to this work.

[2]To whom correspondence should be addressed. Email: jmano@ua.pt.

This article contains supporting information online at www.pnas.org/lookup/suppl/doi:10.1073/pnas.1813336116/-/DCSupplemental.

Published online March 4, 2019.

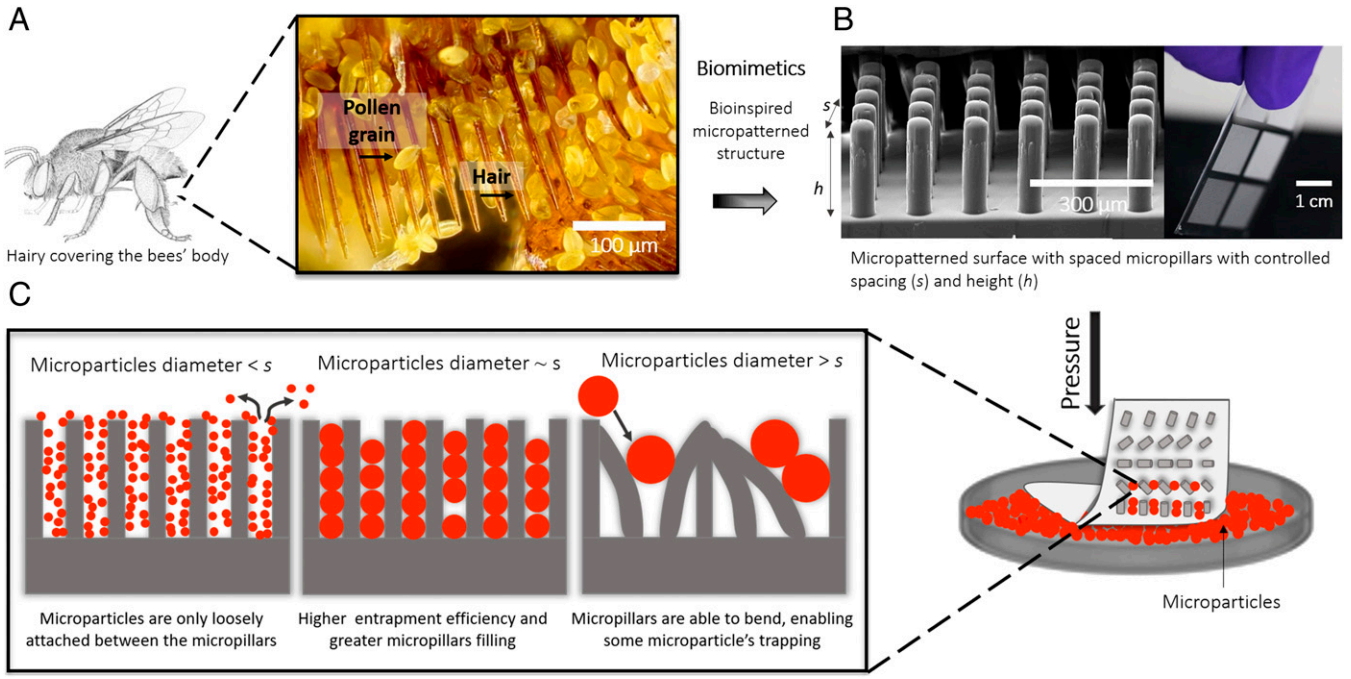

Fig. 1. Schematic illustration of the proposed biomimetic micropatterned structure. (*A*) The bees' body is covered with hairs. Pollen grains are caught between the bees' hair, and their size is similar to the hair spacing. Image courtesy of Charles Krebs (photographer). (*B*) A bioinspired patch can be developed through the construction of a micropatterning structure with micropillars with controlled spacing (*s*) and height (*h*). (*C*) Capture of solid microparticles in a flexible substrate featuring well-organized micropillars by direct contact and pressure; we hypothesized that the entrapment effectiveness will depend on the relationship between the pillar spacing (*s*) and the size of the microparticles.

patches with lower, intermediate, and higher flexibilities with 682 ± 95, 455 ± 39, and 291 ± 42 kPa Young's modulus, respectively, were prepared by a cast molding technique, as briefly detailed in *SI Appendix*, Fig. S1*A*, and were used as a biomimetic substrate for the entrapment of microparticles. Different distances between the micropillars (40, 80 and 160 µm) and different heights of pillars (100 and 300 µm) were tested. *SI Appendix*, Fig. S1*B* shows the silicon wafer used and the resulting patch with two different pillar arrangements (hexagonal and square) (*SI Appendix*, Fig. S1*C*). Side views of the micropillars can be seen in *SI Appendix*, Fig. S1*D*, demonstrating their structural integrity and geometrical fidelity.

Microparticle-Trapping Assays. Different sets of PCL microparticles with diameters matching the micropillar spacings were selected, namely, 40, 80, and 160 µm. The microparticles were produced using an emulsion technique, with the diameters exhibiting a coefficient of variation of 15.8% (*SI Appendix*, Fig. S2). To define the most efficient combination of micropillars and microparticles, trapping assays were performed by simple direct contact of dry microparticles with the patch and the application of a manual pressure (250–2,500 kPa), where microparticles were physically trapped only by friction. Some bending of the surface was also performed to accommodate the maximum amount of particles.

Effect of micropillar spacing. The entrapment effectiveness of each combination is defined as the mass of microparticles entrapped per available area in the patch. Fig. 2 *A*–*C* shows the entrapment effectiveness of microparticles immobilized on the patch with pillars with distinct spacing. Larger quantities of microparticles were found when the particle size was close to the spacing of the pillars, with the available space between micropillars completely occupied. The relative entrapment effectiveness is defined as the volume of entrapped microparticles per available volume within the micropillars in the patch. The relative entrapment effectiveness when the micropillars spacing is similar to microparticles size was superior to 0.8, suggesting a complete filling of the patch (Fig. 2*D*). The entrapment effectiveness as well as the relative entrapment effectiveness of the microparticles in the available space significantly decreased as the difference between the spacing of the micropillars and the size of the microparticles increased. A similar trend was found for all tested combinations, with a large fraction of available space remaining empty for some patches (*SI Appendix*, Fig. S3). These findings are consistent with the initial hypothesis illustrated in Fig. 1*C*. Scanning EM (SEM) micrographs reveal that when the microparticles were smaller than the spacing between the micropillars, they only attached superficially to the microstructures, leaving empty spaces between the micropillars (Fig. 2 *A*–*C*). On the other hand, when the diameter of the microparticles was greater than the micropillar spacing, the microparticles were unable to fit in the space; however, the flexibility of the pillars allowed for a level of particle entrapment, facilitated by the deformation of the vertical structures (more visible in Fig. 2 *A* and *C*). An overview of the effect of micropillar spacing and particle size on entrapment effectiveness is shown in *SI Appendix*, Fig. S4. The number of entrapped microparticles increased as the microparticle diameter decreased. As expected, the larger microparticles occupied the available area with a lower number of microparticles (*SI Appendix*, Fig. S5). We also tested the effect of the geometrical arrangement of the pillars (*SI Appendix*, Fig. S1): for the same spacing, both hexagonal and square geometries led to similar entrapment effectiveness.

Effect of micropillar height. Fig. 2 *A*–*C* and *SI Appendix*, Fig. S3 show greater microparticle entrapment effectiveness for the micropillars 300 µm in height compared with those 100 µm in height for all combinations of particle sizes and pillar spacings studied: $^{****}P < 0.0001$ for 40- and 80-µm microparticle diameter and $^{*}P < 0.05$ for 160-µm microparticle diameter. Patches with the shortest micropillars were only able to entrap a few layers of microparticles, especially for the largest diameter particles (*SI Appendix*, Figs. S6 and S7). Similar to bees' body,

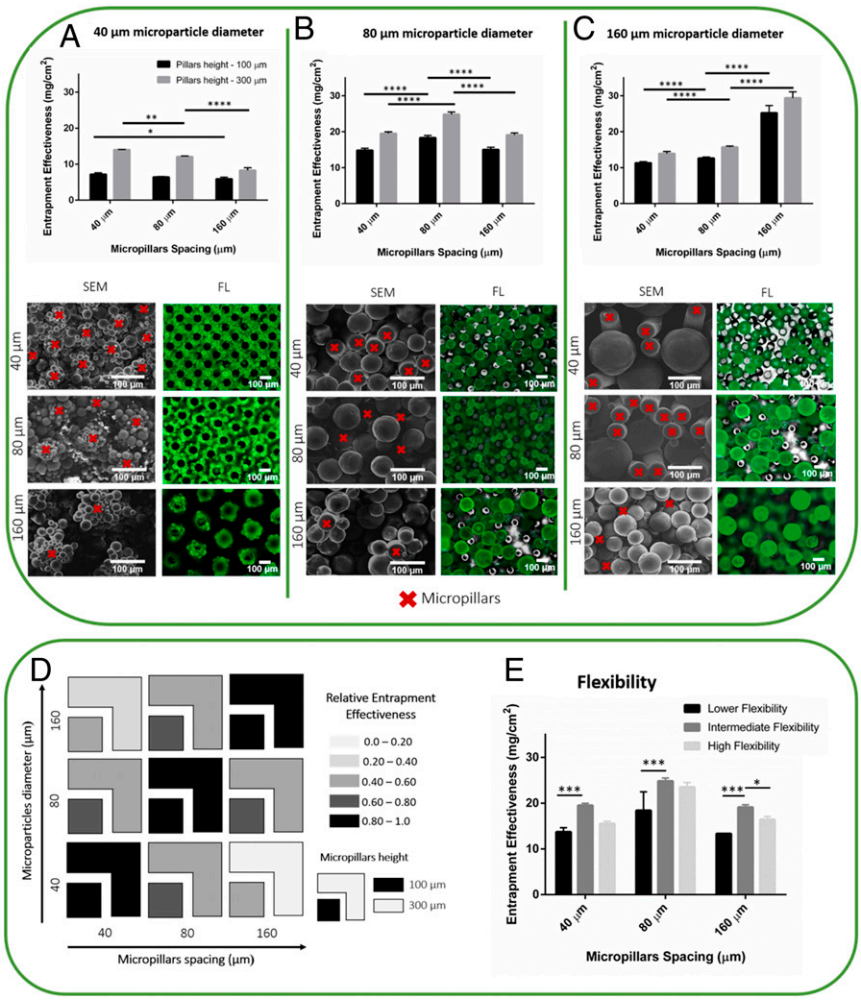

Fig. 2. Entrapment of PCL microparticles within PDMS micropatterning patches. (*A*–*C*) Entrapment effectiveness of microparticles with different diameters: 40 μm (*A*), 80 μm (*B*), and 160 μm (*C*), entrapped within the patches with varying micropillar spacings (40, 80, and 160 μm), micropillar height (100 and 300 μm), and intermediate flexibility. The legend of different pillar heights is represented in the upper right corner of *A*. Coumarin-labeled PCL microparticles were used to visualize the patches by fluorescence microscopy (FL). The micropillars in SEM and fluorescent images of patches with entrapped microparticles are identified in *SI Appendix*, Fig. S8. (*D*) Schematic representation of the relative entrapment effectiveness—volumetric fraction of the microparticles in available volume—of the micropatterned patches after microparticle trapping. (*E*) Entrapment effectiveness of microparticles 80 μm in diameter within patches with 300-μm-high micropillars and variable flexibilities. $*P < 0.05$; $**P < 0.01$; $***P < 0.001$; $****P < 0.0001$.

which presents hairs with a high aspect ratio, taller pillars provided more available space in patch to fix particles.

Effect of patch flexibility. Different patch flexibilities were investigated for entrapping 80-μm microparticles within micropillars 300 μm in height (Fig. 2*E*). *SI Appendix*, Fig. S9 presents the mechanical properties of the fabricated patches. For all flexibilities, the patches with 80-μm spacing were almost completely filled with 80-μm microparticle diameter, with entrapment effectiveness above 20 mg/cm^2 and relative entrapment effectiveness above 0.8. Similar to the body and foreleg hair of bees, which are not rigid structures and bend to accommodate the maximum amount of pollen grains, we envisaged that some patch flexibility would be required to maximize accommodation of microparticles between the pillars. It was found that the patch with intermediate flexibility presented the highest entrapment effectiveness. Of the 54 combinations evaluated in this study, the patches with a microparticle diameter and micropillar spacing of 80 μm (80:80), combined with the tallest micropillars (300 μm) and an intermediate mold flexibility (Young's modulus of 455 ± 39 kPa) (*SI Appendix*, Fig. S9) gave the greatest entrapment effectiveness of 24.8 ± 0.4 mg/cm^2. These patches were therefore selected for the drug-delivery experiments described below.

We hypothesized that the flexibility of the membranes could allow for the release of entrapped microparticles by a simple stretching and shaking mechanism. The average spacing between micropillars would increase due to the increase in strain, leading to a decrease in the mechanical locking effect on the microparticles. A simple qualitative tension assay was performed, resulting in a patch deformation above 100%. Then, a significant amount of entrapped microparticles could be released by a simple mild shaking of the patch. The shaking alone did not dislodge the microparticles that were mechanically locked within the micropillars. Even with flow of compressed air over the membranes, most of the microparticles remained fixed.

Patches for Drug-Delivery Applications. To explore the applicability of the developed biomimetic surface, patches were used to fix solid microparticles for drug-delivery applications. As a proof-of-concept, tetracycline hydrochloride was used in both powder form and encapsulated in alginate hydrogel microparticles to obtain a system with more sustained and controlled drug delivery. In vitro

release studies were performed, and the antibacterial activity of the patch was determined.

Production of tetracycline-loaded alginate microparticles. Spherical alginate microparticles with a diameter of ~80 μm were obtained using electrospraying (*SI Appendix*, Fig. S2 *D* and *E*). To produce tetracycline-loaded alginate microparticles, two different approaches were evaluated (*SI Appendix*, Table S1). The most efficient methodology resulted in a drug content (the percentage of drug in the total mass of microparticles) of 2.10 ± 0.09% and an encapsulation efficiency of 22.7 ± 1.0%, which represents the percentage of drug that was successfully entrapped into the microparticles.

In vitro drug-release studies. Tetracycline-encapsulated alginate particles and bare tetracycline powder with the average size of 80 μm were entrapped in the patches. Tetracycline alginate microparticles alone, i.e., not coupled with patches, were also used to verify the patch interference in the drug release. Both constructs were incubated in PBS at pH 7.4 (physiological environment) and pH 5.5 (simulating the acidic environment of a wound site) (18). The cumulative release profile of the encapsulated drug is depicted in Fig. 3*A*. The total amount of bare tetracycline powder entrapped in the patches was released within 5 min on the solutions of both pH values. However, a more sustained drug-release profile was obtained after the encapsulation of tetracycline in the alginate microparticles. Nevertheless, after 24 h, the percentage of drug released to the medium was similar to the one gathered for the tetracycline alginate microparticles encapsulated in the patches: 68.0 ± 1.2% and 64.8 ± 1.6%, respectively, for pH 5.5; and 72.9 ± 1.7% and 75.5 ± 2.5%, respectively, for pH 7.4. Of note, an initial burst release was observed for these two formulations at both pH values, where at least 50% of the drug content was released within a few minutes.

Antibacterial studies of the prepared dressings. Growth inhibition assays were performed in patches containing bare tetracycline powder or tetracycline alginate particles against both gram-negative and gram-positive bacteria, namely *Escherichia coli* and *Staphylococcus aureus*, to which tetracycline has previously demonstrated an antibacterial activity (19). Furthermore, tetracycline-free patches and patches with tetracycline-free alginate microparticles were used as controls, revealing no evident inhibition zones in both sample formulations (Fig. 3*B*). However, both constructs showed dose-dependent activity against the two distinct bacterial strains after the encapsulation of the tetracycline model drug (Fig. 3*C*). It is noticeable that there is a direct relationship between the drug concentration and the extent of the antibacterial activity. Patches directly exposed to the bare tetracycline powder showed an enhanced antimicrobial activity due the highest drug concentration [100% (wt/wt)] (Fig. 3*C*). Significantly smaller inhibition zones were achieved, for both strains, for patches with tetracycline-encapsulated alginate microparticles, where the drug content within the patch was limited to 2.10 ± 0.09% (wt/wt).

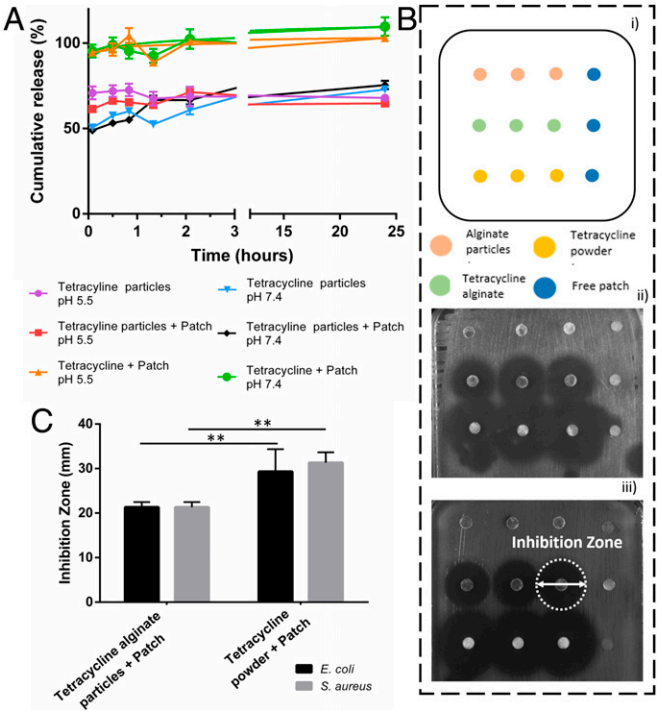

Fig. 3. In vitro release and antimicrobial activity assays from PDMS micropatterned patches. (*A*) In vitro cumulative release of tetracycline from the patches at pH 5.5 and pH 7.4 at 37 °C in PBS. Antimicrobial activity was determined in different combinations: patches alone, patches with nonloaded alginate microparticles, tetracycline-loaded alginate microparticles, or bare tetracycline powder against two microorganisms. (*B*) Antibacterial studies of the prepared patches: distribution of the different combinations of patches on the plate (*i*); antibiogram to gram-negative *E. coli* (*ii*); and antibiogram to gram-positive *S. aureus*, where the dark areas represent the inhibition zone (*iii*). (*C*) Size of the inhibition zone (mm) of the different constructs.

Discussion

Inspired by the ability of the hairy structure present on the legs of bees to entrap millions of pollen grains, we developed a flexible polymer substrate that replicated this extremely efficient system and investigated its ability to entrap microparticles. As hypothesized, the maximum entrapment effectiveness was achieved when the diameter of microparticles matched the spacing between the fabricated micropillars. Of the 54 combinations of different micropillar spacings and heights, microparticle diameters, and patch flexibilities, the patch formulation of 80:80:300 μm (microparticle diameter:micropillar spacing:micropillar height) and intermediate flexibility (455 ± 39 kPa) represented the most effective patch, with an entrapment effectiveness of 24.8 ± 0.4 mg/cm^2. Pollen grains represent up to 30% of bees' bodies. Considering that one bee weights about 90 mg, each bee can carry about 27 mg of pollen grains. Interestedly, this value is very similar to the entrapment effectiveness obtained in the patch herein proposed. Micropillar height had a notable effect on entrapment effectiveness, with the tallest pillars providing a greater volume of space for occupation by particles, mimicking the high-aspect-ratio hairs of honey bees (8). The entrapment effectiveness demonstrated in the current study is significantly higher—about five times more—than those presented by the currently available Food and Drug Administration-approved patches, which deliver drugs such as nicotine, lidocaine, and estradiol at doses around 5.1 mg/cm^2 and range in size from 3.5 to 280 cm^2 (15).

The soft lithography technique employed to fabricate these biomimetic patches is low cost, easy to learn, and accessible to a wide range of users. Furthermore, it can be applied to produce reproducible structures in a wide variety of materials with a range of surface chemistries (20). The substrates herein developed present a simple design and are mechanically resistant, making them particularly suitable for applications where stretching and/or bending are likely to occur.

We also verified that solid drug powder and hydrogel microparticles could be immobilized in the developed bioinspired substrates, to demonstrate the great potential of these systems to be used as patches for drug delivery. Controlled and sustained drug release is required for the treatment of several diseases, including wound healing. Antibiotics, such as tetracycline, have been commonly used during the wound-healing process (21). The incorporation of the drug within the structures of the patch surface allowed for a more controlled release over 24 h, which is in contrast to the bare tetracycline-powder patches, where immediate drug release was observed. The burst release can be easily explained by the probable superficial adsorption of

tetracycline on the alginate microparticles. Owing to the methodology used for drug encapsulation in the present study, it is likely that the tetracycline remained on the outside of the particles, entrapped in the cross-linked network. Also, the low molar mass of tetracycline (444.435 g/mol) may accentuate the concentration gradient and consequently lead to an increase in osmotic pressure, thus causing a burst effect (22). Consequently, when microparticles are placed in contact with an aqueous medium, rapid diffusion is expected to occur.

Burst events followed by a controlled and sustained release of drugs are of particular interest in wound treatment, where an initial burst provides immediate relief followed by prolonged release to promote gradual healing (22). The present findings demonstrate that these patches could be effectively applied either in wound-healing situations or other events that require topical transdermal delivery of a drug. As a proof-of-concept, the constructs showed remarkable antimicrobial activity against both gram-negative and gram-positive bacteria.

The results described herein suggest that the proposed textured surfaces could be further considered for the development of bioinspired devices that entrap and fix large quantities of different microparticles. The fabrication of hairy substrates could be extended to other materials (including biodegradable polymers) and nonflat geometries. One could also envisage the possibility of texturing the lateral surface of the pillars with nano- or submicrometer arrowhead elements to further retain the entrapped particles. Based on the results of this work, patches could be developed for clinical applications, where they could fix a large amount of drug powder or microparticles encapsulating drugs. Such entrapment can be easily accomplished by simple contact of the patch with any powdered product. This could be a valuable solution for the treatment of diseases that require high drug concentrations, enabling less-frequent dosing and thus significantly improving patient compliance. We hypothesize that this system could be appropriate as a platform for the development of a wide variety of micropatterned surfaces for use in applications in the biomedical, biotechnological, environmental, and industrial fields.

Materials and Methods

Materials. All chemicals were purchased from Sigma-Aldrich and used as received, unless otherwise specified. PDMS (Sylgard 184 silicone elastomer kit containing both the base and the curing agent) was purchased from Dow Corning. Silicon masters were obtained by photolithography using a plastic photomask (PhotoData) based on a procedure described elsewhere (23, 24). Masters were then used for the fabrication of PDMS micropatterned patches using soft lithography.

Methods.

PDMS micropatterned patch fabrication. Micropatterned PDMS patches of 1.44 cm^2 in area were obtained through a double-casting process, as previously described (25). Briefly, different silicon wafers were used as masters to obtain patches with different distances between the micropillars (40, 80, and 160 μm) and different pillar heights (100 and 300 μm). Additionally, patches with a range of flexibilities were prepared by using variable base:curing agent ratios, namely, 5:1, 10:1, and 15:1. The Young's modulus of patches with varying flexibilities was determined. The prepared PDMS solutions were then poured onto the patterned silicon wafers and cured at 70 °C for 2 h. To facilitate PDMS-silicon detachment, silicon wafers were pretreated via a silanization protocol. Briefly, the wafers were cleaned with isopropanol, dried in nitrogen, and subsequently treated with ATTO low-pressure plasma system (Diener) for 3–4 min (30 V, 0.6 mbar). The wafers were then immediately placed into a vacuum desiccator containing ∼20 μL/mol of trichloro(1*H*,1*H*,2*H*,2*H*-perfluorooctyl)silane for 2 h (26).

Production of microparticles.

PCL microparticles. An emulsion technique was used to prepare the PCL microparticles (27). PCL was dissolved in dichloromethane [4.5% (wt/vol)] and added dropwise using a 22-gauge needle to a stirring bath (800 rpm) containing [0.5% (wt/vol)] polyvinyl alcohol in water. An OB1 Pressure Controller (Elveflow) was used as the pumping system at 5,000 mbar. After mild stirring to evaporate the organic solvent, the obtained microparticles were subsequently washed with distilled water and collected by centrifugation (200 × *g*, 5 min). Microparticles with different diameter ranges, namely, 25–40 μm, 63–80 μm, and 100–160 μm, were selected with the aid of sieves. To allow better visualization of the entrapment of microparticles within the patches, coumarin-6 was dissolved in acetone (2 mg/mL) and added to the PCL solution. For each 8 mL of PCL, 70 μL of coumarin-6 solution was used. Coumarin–PCL microparticles were produced following the same protocol as described for the plain PCL microparticles.

Tetracycline-loaded alginate microparticles. Alginate microparticles were produced using an electrospraying technique (SprayBase; Avectas). First, microparticles with and without tetracycline were optimized to obtain a rounded shape and a diameter of 80 μm. The flow rate was set to 1.0 mL/h, and the needle-to-collector distance was set at 6 cm. To optimize the encapsulation of tetracycline, which represents the percentage of drug that was successfully entrapped into the microparticles, two different methodologies were employed. For tetracycline-free microparticles, a needle diameter of 22 gauge was used with an alginate concentration of 2.0% wt/vol and 10 kV voltage. For tetracycline-encapsulated microparticles, the needle diameter and the polymer concentration were decreased to 26 gauge and 1.75% (wt/vol), respectively, and the voltage was increased to 15 kV. A solution of calcium chloride (0.1 M) was used as a cross-linking bath under continuous agitation (300 rpm). In a subsequent experiment, alginate microparticles (10 mg) obtained using the electrospray technique were freeze-dried and then suspended in 5 mL of tetracycline solution. The suspension was allowed to stir at room temperature for 24 h and then was again freeze-dried (28, 29). The amount of tetracycline encapsulated was determined by de-cross-linking the alginate microparticles in EDTA (0.1 M) solution.

Tetracycline-powder microparticles. Tetracycline-powder microparticles were obtained by milling tetracycline hydrochloride with the aid of a mortar with agate pestle. The obtained microparticles were then separated into diameter ranges of 25–40 μm, 63–80 μm, and 100–160 μm using sieves.

Microparticle entrapment into patches. The different patches were pressed against the produced PCL or alginate microparticles to promote their capture. To evaluate the entrapment effectiveness, the different formulations of the patches entrapping different microparticles were weighed. The entrapment effectiveness was defined as the mass of microparticles entrapped in the available space of the patches. Additionally, relative entrapment effectiveness was also established as the ratio between the volume occupied by the entrapped microparticles and the available volume in the patch. The available volume in the patches was defined by $h \times$ available area, where h is the height of the pillars and the available area represents the area of the patch that is not occupied by the pillars. Additionally, the volume occupied by entrapped microparticles was determined as the ratio between the mass of entrapped microparticles and the volumetric mass density of PCL (1.145 g/cm^3).

PDMS micropatterned patch characterization. The surface of the patches either with or without PCL microparticles was visualized by SEM (S4100; Hitachi). The samples were gold sputter-coated using an accelerating voltage of 25 kV. Patches entrapping coumarin–PCL microparticles were accessed by EGFP fluorescence microscopy (Zeiss Imager M2; Zeiss).

The mechanical behavior of different patches was characterized through tensile testing (MMT-101N; Shimazdu Scientific Instruments) with a load cell of 100 N and a velocity of 1 mm/min. Patches alone or with entrapped PCL microparticles were tested ($n = 3$). The sample thickness was measured using a micrometer with a precision of 1 μm. For each sample, the load versus cross-head displacement data from initial until rupture load were measured using a computer data acquisition system connected to the tester. The initial gauge length was set to 8 mm.

In vitro drug-release studies. Patches with 80:80:300 μm (microparticle diameter:micropillar spacing:micropillar height) and with intermediate flexibility were prepared and the controlled release of tetracycline assessed. The in vitro release assays were performed in PBS solutions at both physiological pH (7.4) and wound pH (5.5) (18). The drug release from patches enclosing tetracycline-encapsulated alginate microparticles or bare tetracycline-powder microparticles was evaluated. Tetracycline-free alginate microparticles and patches without entrapped microparticles were used as controls. Briefly, the samples were immersed in 5 mL of PBS and subsequently stirred in a shaking water bath at 60 rpm and 37 °C. Then, at predetermined time points, aliquots of 500 μL of PBS were withdrawn, and the same volume was replaced with fresh buffer solution. The tetracycline concentration of each aliquot was quantified by UV-visible (UV-vis) spectrometry at 362 nm in a microplate reader (Synergy HTX; BioTek Intruments) using a Corning 384-well quartz microplate (Hellma) (29). The cumulative release of tetracycline was calculated according to the Hailong equation, as follows (30):

$$\text{Cumulative tetracycline release profile}(\%) = \frac{V_e \sum_i^{n-1} c_i + V_0 c_n}{m_{tetracycline}} \times 100.$$

Growth-inhibition assay. The ability of the patches (6 mm in diameter) presenting tetracycline-encapsulated alginate microparticles and bare tetracycline-powder microparticles to inhibit bacterial growth was investigated using *E. coli* [American Type Culture Collection (ATCC)] and *S. aureus* (ATCC) cultures. Patches without entrapped microparticles and those encapsulated with tetracycline-free alginate microparticles were used as control formulations. Bacterial colonies isolated from nutrient agar were prepared by inoculating them into 5 mL of LB medium (Merck), followed by incubation for 18–24 h in a shaking water bath at 180 rpm and at 37 °C. Then, the obtained bacteria cellular suspensions (1 mL) were centrifuged at 13,000 × *g* for 10 min, the supernatant was discarded, and the resulting pellet suspension was resuspended in an aqueous sodium chloride solution [0.9% (wt/vol)]. The cellular density was determined by UV-vis spectrometry at 600 nm (UV mini-1240 UV-VIS Spectrophotometer; Shimadzu). After inoculum spreading in Mueller Hinton agar medium (nzytech), the samples were incubated at 37 °C for 24 h, as described elsewhere (31). The diameters of the inhibition zones around the patches were subsequently measured manually. Each disk diffusion test was repeated three times.

Statistics. All statistical analysis was performed using GraphPad with two-way ANOVA followed by the Bonferroni post hoc test, with a significance level set at $P < 0.05$.

ACKNOWLEDGMENTS. We thank the initial support from Dr. João Gaspar (International Iberian Nanotechnology Laboratory) in the preparation of the silicon micromolds. We also acknowledge the support from Prof. Isabel Henriques (Centre for Environmental and Marine Studies) in the development of the antimicrobial assays. We acknowledge the project CICECO–Aveiro Institute of Materials, POCI-01-0145-FEDER-007679 [Fundação para a Ciência e Tecnologia (FCT) Ref. UID/CTM/50011/2013], financed by national funds through the FCT/Ministério da Educação e Ciência. This work was supported by project ATLAS of the European Research Council Grant Agreement ERC-2014-ADG-669858 (to J.F.M.). This work was also financed by Postdoctoral Grants BPD/UI89/7350/2017 (to C.R.C.) and BPD/UI89/7429/2016 (to A.S.S.) and Research Grant BI/UI89/8057/2018 (to L.F.S.).

1. Sanchez C, Arribart H, Guille MM (2005) Biomimetism and bioinspiration as tools for the design of innovative materials and systems. *Nat Mater* 4:277–288.
2. Bhushan B (2009) Biomimetics: Lessons from nature–An overview. *Philos Trans A Math Phys Eng Sci* 367:1445–1486.
3. Nishimoto S, Bhushan B (2013) Bioinspired self-cleaning surfaces with superhydrophobicity, superoleophobicity, and superhydrophilicity. *RSC Adv* 3:671–690.
4. Cleymand F, Rousseau M, Mano JF (2015) Introducing biomimetic approaches to materials development and product design for engineering students. *Bioinspired Biomimetic Nanobiomater* 4:207–212.
5. Hancock MJ, Sekeroglu K, Demirel MC (2012) Bioinspired directional surfaces for adhesion, wetting, and transport. *Adv Funct Mater* 22:2223–2234.
6. Reddy S, Arzt E, del Campo A (2007) A. Bioinspired surfaces with switchable adhesion. *Adv Mater* 19:3833–3837.
7. Gorb SN, Sinha M, Peressadko A, Daltorio KA, Quinn RD (2007) Insects did it first: A micropatterned adhesive tape for robotic applications. *Bioinspir Biomim* 2:S117–S125.
8. Amador GJ, et al. (2017) Honey bee hairs and pollenkitt are essential for pollen capture and removal. *Bioinspir Biomim* 12:026015.
9. Lin H, Qu Z, Meredith JC (2016) Pressure sensitive microparticle adhesion through biomimicry of the pollen-stigma interaction. *Soft Matter* 12:2965–2975.
10. Casteel D (1912) *The Behavior of the Honey Bee in Pollen Collection* (Department of Agriculture, Bureau of Entomology, Washington, DC), Bulletin No. 121; reprinted (2012) (Library of Alexandria, Alexandria, Egypt), pp 1–69.
11. Allen TM, Cullis PR (2004) Drug delivery systems: Entering the mainstream. *Science* 303:1818–1822.
12. Wiedersberg S, Guy RH (2014) Transdermal drug delivery: 30+ years of war and still fighting! *J Control Release* 190:150–156.
13. Prausnitz MR, Langer R (2008) Transdermal drug delivery. *Nat Biotechnol* 26:1261–1268.
14. Brown MB, Martin GP, Jones SA, Akomeah FK (2006) Dermal and transdermal drug delivery systems: Current and future prospects. *Drug Deliv* 13:175–187.
15. Santos LF, Correia IJ, Silva AS, Mano JF (2018) Biomaterials for drug delivery patches. *Eur J Pharm Sci* 118:49–66.
16. Naik A, Kalia YN, Guy RH (2000) Transdermal drug delivery: Overcoming the skin's barrier function. *Pharm Sci Technol Today* 3:318–326.
17. Ruhe JJ, Menon A (2007) Tetracyclines as an oral treatment option for patients with community onset skin and soft tissue infections caused by methicillin-resistant Staphylococcus aureus. *Antimicrob Agents Chemother* 51:3298–3303.
18. Schneider LA, Korber A, Grabbe S, Dissemond J (2007) Influence of pH on wound-healing: A new perspective for wound-therapy? *Arch Dermatol Res* 298:413–420.
19. Shahverdi AR, Fakhimi A, Shahverdi HR, Minaian S (2007) Synthesis and effect of silver nanoparticles on the antibacterial activity of different antibiotics against Staphylococcus aureus and Escherichia coli. *Nanomedicine* 3:168–171.
20. Qin D, Xia Y, Whitesides GM (2010) Soft lithography for micro- and nanoscale patterning. *Nat Protoc* 5:491–502.
21. Martin P (1997) Wound healing–Aiming for perfect skin regeneration. *Science* 276:75–81.
22. Huang X, Brazel CS (2001) On the importance and mechanisms of burst release in matrix-controlled drug delivery systems. *J Control Release* 73:121–136.
23. Kantak C, Beyer S, Yobas L, Bansal T, Trau D (2011) A 'microfluidic pinball' for on-chip generation of layer-by-layer polyelectrolyte microcapsules. *Lab Chip* 11:1030–1035.
24. Yang IH, Co CC, Ho C-C (2005) Alteration of human neuroblastoma cell morphology and neurite extension with micropatterns. *Biomaterials* 26:6599–6609.
25. Gitlin L, Schulze P, Belder D (2009) Rapid replication of master structures by double casting with PDMS. *Lab Chip* 9:3000–3002.
26. Théry M, Piel M (2009) Adhesive micropatterns for cells: A microcontact printing protocol. *Cold Spring Harb Protoc* 2009:pdb.prot5255.
27. Luciani A, Coccoli V, Orsi S, Ambrosio L, Netti PA (2008) PCL microspheres based functional scaffolds by bottom-up approach with predefined microstructural properties and release profiles. *Biomaterials* 29:4800–4807.
28. Correia CR, Reis RL, Mano JF (2013) Multilayered hierarchical capsules providing cell adhesion sites. *Biomacromolecules* 14:743–751.
29. Silva AS, et al. (2017) Aerosolizable gold nano-in-micro dry powder formulations for theragnosis and lung delivery. *Int J Pharm* 519:240–249.
30. Che H, et al. (2015) CO_2-switchable drug release from magneto-polymeric nanohybrids. *Polym Chem* 6:2319–2326.
31. Siafaka PI, Zisi AP, Exindari MK, Karantas ID, Bikiaris DN (2016) Porous dressings of modified chitosan with poly(2-hydroxyethyl acrylate) for topical wound delivery of levofloxacin. *Carbohydr Polym* 143:90–99.